

A modeling study on the effects of MJO and equatorial Rossby waves on tropical cyclone genesis over the western North Pacific in June 2004



Lin Ching^a, Chung-Hsiung Sui^{a,*}, Ming-Jen Yang^a, Pay-Liam Lin^b

^a Department of Atmospheric Sciences, National Taiwan University, Taiwan

^b Department of Atmospheric Sciences, National Central University, Taiwan

ARTICLE INFO

Article history:

Received 7 July 2015

Received in revised form

24 September 2015

Accepted 8 October 2015

Available online 17 October 2015

Keywords:

MJO

Rossby wave

Tropical cyclogenesis

WRF

Numerical simulation

ABSTRACT

This study investigates the influence of the Madden Julian oscillations (MJO) and equatorial Rossby (ER) waves on tropical cyclone (TC) formation in western Pacific during June 2004 through one control and three wave experiments for each of the five TCs. The control experiment reasonably simulates the formation of five TCs. In the corresponding wave experiments, the MJO, ER waves, and both the MJO and ER waves are removed, from the initial fields and lateral boundary conditions, respectively. The differences of simulated TC intensity between the control and corresponding wave experiments provide a quantitative assessment of the relative contribution of each wave to TC formation.

In the wave experiments with the MJO removed, three of the five TCs are weakened, and the remaining two (TC A and B) grow stronger due to an altered background flow that steered the TCs into more favorable oceanic regions. For the wave experiments with ER waves removed, three of the five simulated TCs become weaker (TC A, C, and E). TC D develops into a tropical storm because of a dominant influence from active synoptic-scale disturbance. The results indicate that both the MJO and ER waves have an important modulating effect on TC formation. In addition to the influence from the MJO, ER and synoptic-scale waves, local processes may dominate in TC formation; for the example of TC B, none of the waves positively influence the formation in significant ways. The present modeling approach provides a quantitative assessment of the relative contribution of tropical wave disturbances to TC formation.

© 2015 Elsevier B.V. All rights reserved.

1. Introduction

Since the discovery of equatorially trapped waves in the 1960s (Matsuno, 1966; Yanai and Maruyama, 1966; Lindzen, 1967; Wallace and Kousky, 1968), observational studies show that tropical waves in the troposphere are coupled with convection, and their space-time spectra fit the dispersion relation from the linear wave theory (Takayabu and Nitta, 1994; Wheeler and Kiladis, 1999; Roundy and Frank, 2004). In addition to the convection-coupled waves, other wave activities at synoptic and intraseasonal scales are also observed in the tropical troposphere. These tropical wave disturbances are especially active in the western North Pacific (WNP) region where the Pacific warm pool and the summer monsoon provide

* Corresponding author.

E-mail address: sui@as.ntu.edu.tw (C.-H. Sui).

a favorable background for the development of multi-scale disturbances. The intraseasonal oscillations (ISOs) observed in WNP bear basic wave structures of the Madden–Julian oscillation (MJO; Madden and Julian, 1971) but with more complex northward propagating signals (Lau and Chan, 1986; Wang and Rui, 1990; Hendon and Salby, 1994). Previous studies also found that the WNP is rich in synoptic wave trains in boreal summer (Reed and Recker, 1971; Lau and Lau, 1990, 1992; Chang et al., 1996). This synoptic wave train is sometimes called a tropical depression (TD)-type disturbance. Some of the TD-type disturbances are found to develop from a westward-propagating mixed Rossby-gravity (MRG) wave into a zonal wind convergence region (Takayabu and Nitta, 1993; Dickinson and Molinari, 2002). The possible origins of synoptic wave trains are discussed in Li (2006) and references therein.

WNP is rich not only in multi-scale waves but also in tropical cyclones (TCs), as shown in many previous studies. Liebmann et al. (1994) examined the connection between the MJO and TCs in the western Pacific and Indian oceans and found that TCs preferentially occur in the MJO-related convective region. Kim et al. (2008) showed that the number of TC genesis increases when the MJO-related convective region moves into the WNP and the genesis region follows the propagation of the MJO-related convective region. Hsu et al. (2011) showed that the genesis number and location and intensification rate of TCs in the WNP are closely related to the barotropic energy conversion. Hsu and Li (2011) also indicated that the eddy momentum transport may contribute to the northward propagation of the boreal summer ISO over the WNP. Yamazaki and Murakami (1989) found that tropical cyclogenesis over the WNP is related to the amplitude of 20–40-day westward-propagating waves in the meridional direction averaged between 6° N and 16° N. The characteristics of such waves are consistent with the $n = 1$ equatorial Rossby (ER) waves. Numaguti (1995) investigated the formation of six TCs in the western Pacific during the Tropical Ocean Global Atmosphere Coupled Ocean-Atmosphere Response Experiment (TOGA COARE). He suggested that all six genesis cases are associated with MRG or ER waves. Frank and Roundy (2006) showed that TCs developed in the presence of enhanced activity of MRG and ER waves. Fu et al. (2007) analyzed 34 TC genesis events in the WNP during the 2000 and 2001 typhoon seasons. They showed three types of synoptic-scale disturbances are identified in the pregenesis stages, which are tropical cyclone energy dispersions, synoptic wave trains (SWT), and easterly waves. Li (2012) summarized synoptic and climate aspects of TC genesis in the WNP. They indicated that synoptic-scale disturbances or intraseasonal oscillation can lead to individual TC genesis events. Molinari et al. (2007) studied the tropical cyclogenesis within an ER wave packet and constructed a composite around the genesis location. Their composite showed that TCs form east of the cyclonic center of composite ER wave, which is in a region of strong convection and a separate 850-hPa vorticity maximum. Their results are consistent with the composite of Frank and Roundy (2006) and the numerical simulation of Gall et al. (2010). Dickinson and Molinari (2002) performed a case study to show that westward-propagating MRG wave and TD-type disturbance (hereafter MRG–TD) can supply precursor disturbances for repeated formation of TCs. They also pointed out that the TCs do not form in the center of the lows, but to their east, where the maximum convergence of linear MRG wave solution occurred. Chen and Tam (2012) pointed out that tropical cyclogenesis can excite equatorial MRG wave through southeastward energy dispersion.

The influence of the quasi-biweekly gyre and low-frequency monsoon flows on the slow movement and asymmetric precipitation of Typhoon Morakot (2009) was emphasized in observational (Wu et al., 2011) and modeling (Liang et al., 2011) studies. Liang et al. (2011) performed numerical experiments to investigate the influences of multi-time-scale monsoonal flows on the track change of Typhoon Morakot. They temporally filtered the initial fields and lateral boundary conditions to remove selected spectra to show that the interaction between TCs and low-frequency monsoon gyres can cause sudden changes in TC tracks. Cao et al. (2014) investigated the effects of ISO of Monsoon trough on TC formation by using the Weather Research and Forecasting (WRF) Model. They showed that the ISO can influence TC formation through both dynamic and thermodynamic processes. Xu et al. (2014) also used the WRF Model to investigate the effects of multiscale motions on the genesis of Typhoon Manyi (2001). In the absence of SWT-ISO-scale interaction, the southeastward energy dispersion was weakened significantly and the disturbance would not develop into a TC.

Despite the above studies, the process for TCs to form in multi-scale background flow is still not well understood in the WNP due to the complicated nature of the problem. In our previous study (Ching et al., 2010; hereafter CSY10), the climate background of TC genesis in June 2004 was examined. We investigated causal relations between the tropical wave disturbances and TC formation in CSY10 by analyzing the structure of equatorial waves and corresponding vorticity at the TC warning time. According to the analysis in CSY10, a more definitive study of the effect of large-scale waves on TC formation can be made by isolating the contribution of each wave to TC formation during the developing period of initial disturbance. The above considerations are the primary motivation for the current modeling study.

The rest of this paper is organized as follows. Section 2 describes the data and experiments design. The results of simulated TC formation compared with observations are shown in Section 3. Section 4 indicates the effects of the MJO and ER waves on TC formation. Finally, summary and discussion are presented in Section 5.

2. Data and experiments design

This study uses the 6-hourly analysis data obtained from the global assimilation data produced by the National Centers for the Environmental Prediction (NCEP) Global Data Assimilation System (GDAS) that has been archived at National Climatic Data Center back to 1997 (Kanamitsu, 1989). The NCEP GDAS is the final run in the series of NCEP operational runs. NCEP post-processing of GDAS converts the data from the spectral coefficient at sigma levels to 1° latitude-longitude grid at mandatory pressure levels. This 6-hourly final (FNL) gridded analysis data is utilized to analyze the detailed structure of waves and TCs

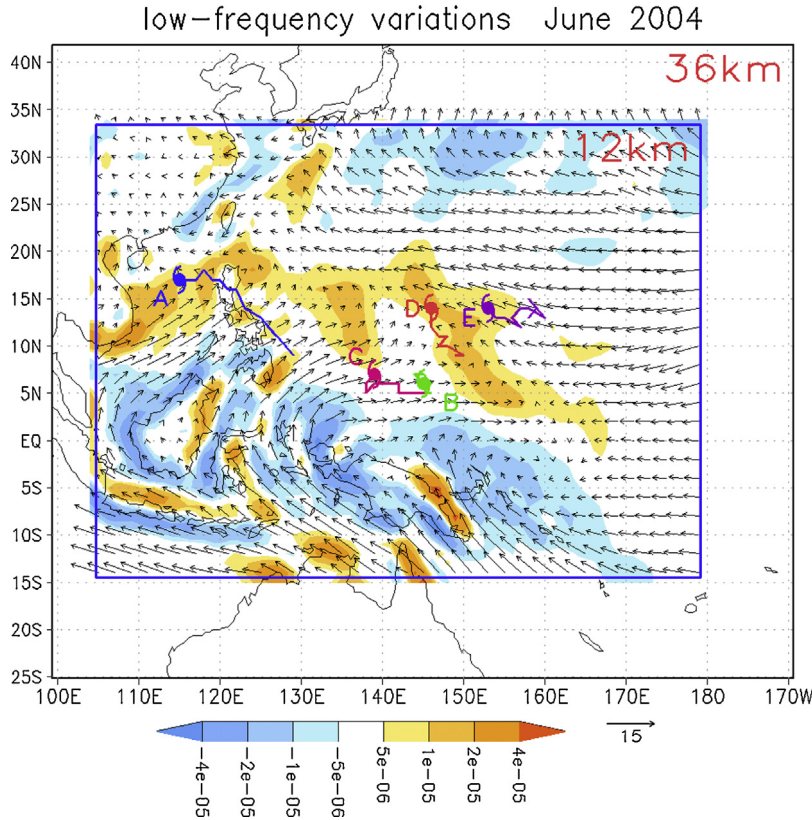


Fig. 1. The double-nested domains used in the ARW-WRF simulation with 36-, and 12-km grid sizes. The combined vorticity (color shaded, in s^{-1}) and winds (vector, in $m s^{-1}$) at 850 hPa in the inner domain combine the monthly mean fields of climatology, interannual, and the MJO variations, for June 2004. The sequence of genesis are represented by the genesis location of TC A–E shown by the typhoon symbols and the tracks of each initial disturbance prior to the warning time.

during the month of June 2004. The daily interpolated outgoing longwave radiation (OLR; Liebmann and Smith, 1996) is used as a proxy for deep tropical convection. This data is obtained from the National Oceanic and Atmospheric Administration (NOAA) polar orbiting satellites.

The best track information of TCs is produced by the Joint Typhoon Warning Center (JTWC) and updated every six hours. The JTWC best tracks are post-analyzed tracks and are point estimates of minimum sea level pressure (SLP) and maximum sustained winds. The warning time of each TC is defined as the time when it first attained tropical depression stage according to the JTWC best track data.

In order to isolate individual equatorial wave mode, Wheeler and Kiladis (1999) developed a wavenumber–frequency spectral analysis to identify the zonally propagating tropical waves. We perform a wavenumber–frequency spectral analysis on OLR, zonal and meridional winds, temperature, humidity, and height fields to extract the MJO, ER waves, and MRG-TD waves for an entire year (2004). The wavenumber and frequency of each wave are referred to Frank and Roundy (2006). The MJO signal is extracted by retaining only those eastward-moving spectral components that correspond to waves with zonal wavenumbers of 0–5 and periods of 30–90 days. The ER waves correspond to westward-moving components with zonal wavenumbers of 1–10 and periods of 10–40 days. The MRG-TD waves correspond to westward-moving components with zonal wave numbers of 0–14 and periods of 2.5–10 days. Schreck et al. (2011) pointed out that the influence of TCs on the equatorial wave spectrum is generally small. The exception occurs in shorter-wavelength westward-propagating waves, which correspond to the MRG-TD wave disturbances. Because the MRG-TD wave is hard to separate from TCs, the MRG-TD wave experiments are not considered in present study.

In CSY10, we defined a wave-related (WR) index within the $5^\circ \times 5^\circ$ box surrounding a TC center to determine the relation between major tropical waves and TC formation. The area-mean value of the OLR and vorticity fields of each wave on the cyclone center is normalized by the corresponding standard deviation, which is calculated by all 25 months of June. The WR index is defined as the sum of the normalized vorticity and the normalized value of the reversed OLR. The large positive WR index means that the wave is significant on the cyclone center.

The Advanced Research Weather Research and Forecasting (WRF) modeling system is adopted in this study. The numerical simulations include two domains with horizontal grid sizes of 36- and 12-km (Fig. 1). The outer and inner domains cover the regions of $25.2^\circ S$ – $41.8^\circ N$, 99.3° – $190.7^\circ E$ and $16.5^\circ S$ – $33.4^\circ N$, 106.2° – $177.7^\circ E$, respectively. Thirty-five levels are used

Table 1

Descriptions of numerical experiments.

Experiment	Initial fields and lateral boundary conditions
CTL	Unfiltered NCEP FNL analysis data
noMJO	Analysis data excluding the MJO
noER	Analysis data excluding Rossby waves
noMJOER	Analysis data excluding the MJO and Rossby waves together

in the vertical with a top of 10 hPa. The WRF single-moment (WSM) six-class microphysics scheme (Hong and Lim, 2006) is used for cloud microphysics scheme. The Grell 3D ensemble convective scheme (Grell and Devenyi, 2002) is only used in the outer domain. No cumulus scheme is adopted in the inner domain. The Mellor-Yamada-Janjić (Janjić, 2002) is used for the planetary boundary layer parameterization scheme. The Rapid Radiative Transfer Model (RTTM) longwave parameterization (Mlawer et al., 1997) and the Dudhia shortwave parameterization (Dudhia, 1989) are used for the radiation calculation. The NCEP FNL analysis data were used to initialize the ARW-WRF model. No TC initialization scheme is used. Only the results of inner domain are discussed in present study.

In order to estimate the contribution of tropical waves to the formation of the 5 TCs during the study period, we trace each TC back in time from the warning time to an initial state when the vorticity, averaged in a $5^\circ \times 5^\circ$ box surrounding the disturbance center, is less than the Coriolis frequency at the related latitude or when there is no identifiable closed circulation. The formation period (tracing time) for TC A to TC E are 84, 54, 60, 48, and 66 h, respectively, and the corresponding tracks are shown in Fig. 1. The initial disturbance of TC A moves a long distance from the Philippine Sea to the South China Sea (SCS) while the initial disturbance of TC B is almost stationary at 145° E, 6° N. The initial disturbances of the rest three TCs (TC C, D, and E) can be traced to 138° – 145° E, 150° E, and 160° E, respectively, within the 6° – 15° N latitude band. Each simulation starts with a six-hour spin-up time before the formation period and ends two days after the warning time. The simulation time for TC A to TC E are 138, 108, 114, 102, and 120 h, respectively. For each TC, we perform four experiments: a control experiment (CTL) and three wave experiments (Table 1). The CTL is performed with unfiltered analysis data for initial fields and lateral boundary conditions. For the three wave experiments, kinetic (winds) and thermodynamic (temperature, humidity, and height) fields associated with the MJO, ER waves, and both the MJO and ER waves are respectively removed from the initial fields and lateral boundary conditions at all vertical levels. The three experiments are referred to as noMJO, noER, and noMJOER, respectively, in the following discussion. The simulations are designed to determine the different intensities of simulated TCs between the CTL and each wave experiment to assess the contribution of the wave on TC formation. Before the discussion of numerical experiments, a sensitive test was used to clarify the influence of kinetic and thermodynamic fields on our wave experiments (see Appendix I). We also examine the space-time filtered wave structure carefully to make sure that the kinetic and thermodynamic fields of the filtered waves maintain mutual physically-coherent structure. This is done by comparing the space-time filtered height field (H_f) with the balanced height field (H_b) that is calculated from space-time filtered wind fields based on the nonlinear balance equation (see Appendix II). The difference between H_f and H_b is small, indicating that the space-time filtering mostly preserve the nonlinear balance relation. But the difference between H_f and H_b is further compared with the space-time filtered divergent winds and divergence fields to show that their features are consistent with the MJO and ER waves structures. Both balanced and imbalanced fields are important for driving the TC genesis, and it is essential that the balance between kinetic and thermodynamic fields of waves are preserved by space-time filtering in numerical experiments.

3. Simulated TC formation compared with observations

In the WNP, June is normally a transition month to the typhoon season, and therefore sensitive to climate oscillations. CSY10 showed that the month of June 2004 is in the developing stage of a warm (El Niño) episode and a strong convective phase of the MJO. Associated with the favorable climate background, multi-scale waves are also active in June 2004. To further show the spatial patterns of the large-scale background flow and waves at the warning times of the five TCs, we show in Fig. 2 the height fields and total winds at 850 hPa, and in Fig. 3 the space-time filtered winds and vorticity fields at 850 hPa for ER waves along with the negative OLR regions of the MJO represented by red contours. Fig. 2 indicates that easterlies dominate the WNP and westerlies exist around the Equator in early June. The westerly winds move north-eastward and are strengthened in late June (Fig. 2d and e). The north-eastward propagating westerlies represent the MJO convective phase (Figs. 2 and 3). ER waves are characterized by NE-SW oriented cyclonic and anticyclonic circulation moving west-northwestward. The MJO and ER waves are important large-scale disturbances favorable for TC formation to be discussed below.

In order to assess the influences of individual wave on TC formation, we show in Fig. 4 the simulated winds and height fields at 850 hPa from the CTL for the five TCs. The observed results at the warning times of each of the five TCs are reasonably simulated by the CTL. The simulated location of TC A forms east of the observed location due to the stronger simulated southwesterlies (Fig. 4a and Fig. 2a), which takes more time to pass Philippines (Fig. 1). But the disturbance of TC A still grows into a tropical storm (TS). The formation of TC B is successfully simulated as shown by the circulation of TC B in the CTL, as

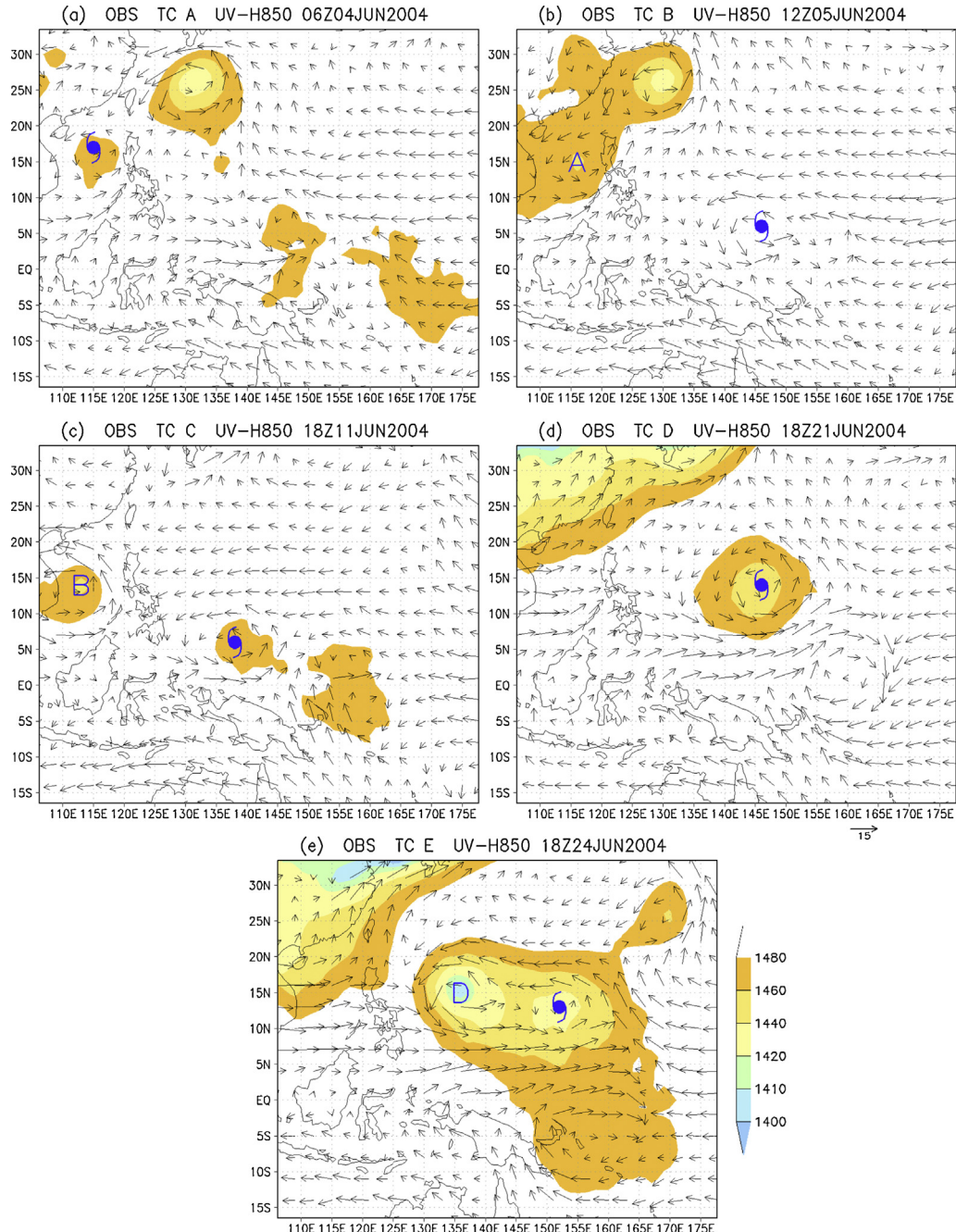


Fig. 2. The observed fields of total winds (vector, in m s^{-1}) and height (color shaded, in m) at 850 hPa at the warning time of (a) TC A, (b) TC B, (c) TC C, (d) TC D, and (e) TC E. The genesis locations are indicated by the Typhoon symbols and corresponding letters, respectively. The letter A, B, and D refer to TC A, TC B, and TC D, respectively. (For interpretation of the references to color in this figure legend, the reader is referred to the web version of this article.)

comparing with the observed circulation (Fig. 4b and Fig. 2b). The circulations of TC A and another cyclone east of Taiwan are also well simulated. The simulated circulation of TC C at formation time is shown in Fig. 4c. The simulated anticyclone southeast of TC C is stronger than the observed. The observed TC D and the TD-type disturbance are reproduced in the CTL (Fig. 4d and Fig. 2d), but with a slightly stronger TC circulation and westerlies in the Philippine Sea. The simulated center of TC E is about 14° east-southeast of TC D in the CTL, while the corresponding distance in observation is 16° (Fig. 4e and Fig. 2e). The simulated circulation of TC E is slightly stronger than in observation, but the circulation of TC D is weaker. The CTL also shows an ER wave structure consistent with the observation.

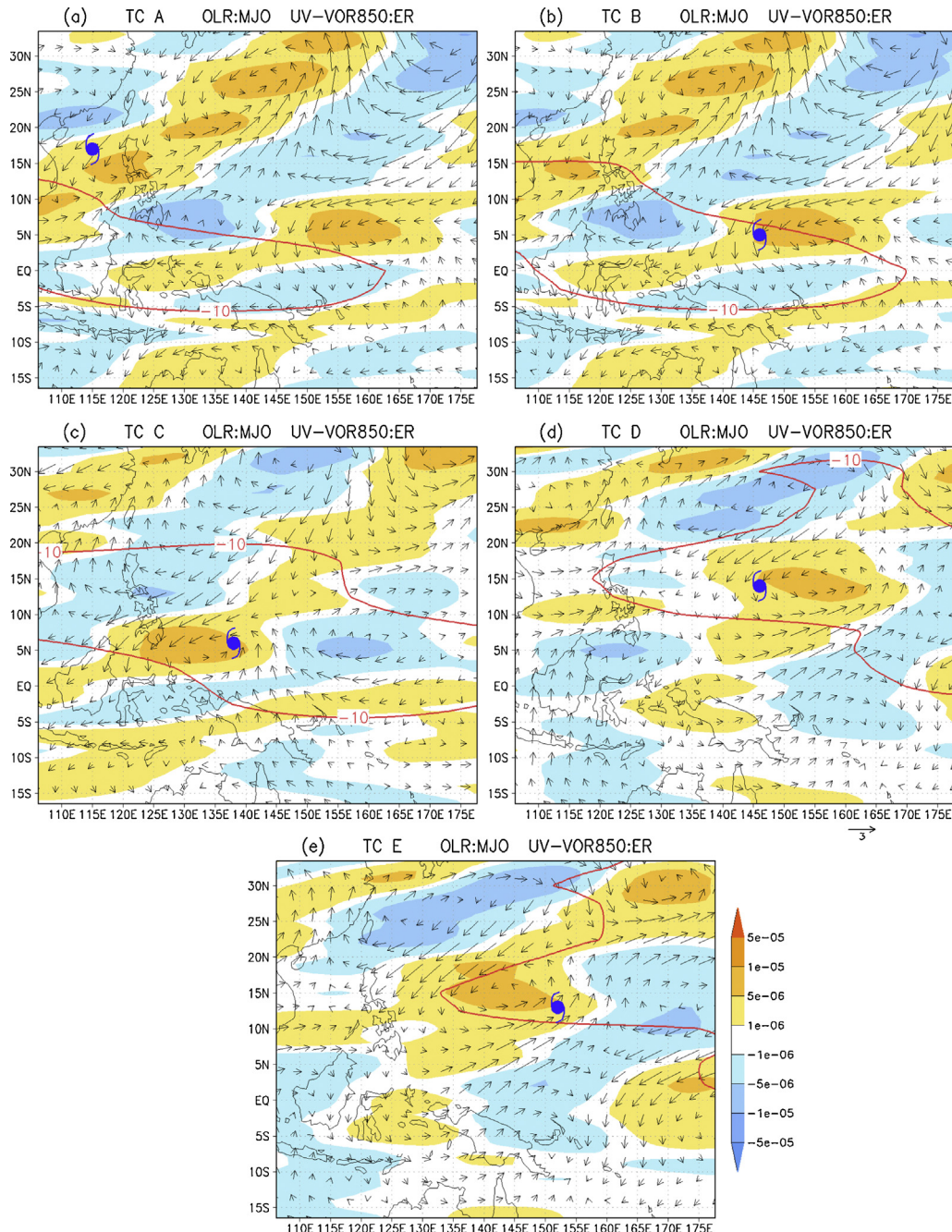


Fig. 3. Same as Fig. 2, but for the space-time filtered winds (vector, in m s^{-1}) and vorticity (color shaded, in s^{-1}) of ER waves at 850 hPa along with the negative OLR regions of the MJO shown by the red contour. Only the OLR value of -10 W m^{-2} is plotted. (For interpretation of the references to color in this figure legend, the reader is referred to the web version of this article.)

4. Effects of the MJO and ER waves on TC formation

In CSY10, we had computed the sum of the normalized OLR and vorticity as a wave related (WR) index to consider the contribution by both vorticity and divergence fields and had discussed the results of WR indexes at the warning time of five TCs. In the current study, we extended the period of WR index to examine the contribution of each wave during the development periods of the five TCs. The mean WR indexes of three waves (MJO, ER, and MRG-TD) two days before and after the warning time are shown in Table 2. The mean WR indexes two days before the warning time (the developing stage) of TC A show that the contributions of the MJO and the MRG-TD wave are negative. ER wave is the main wave related to the

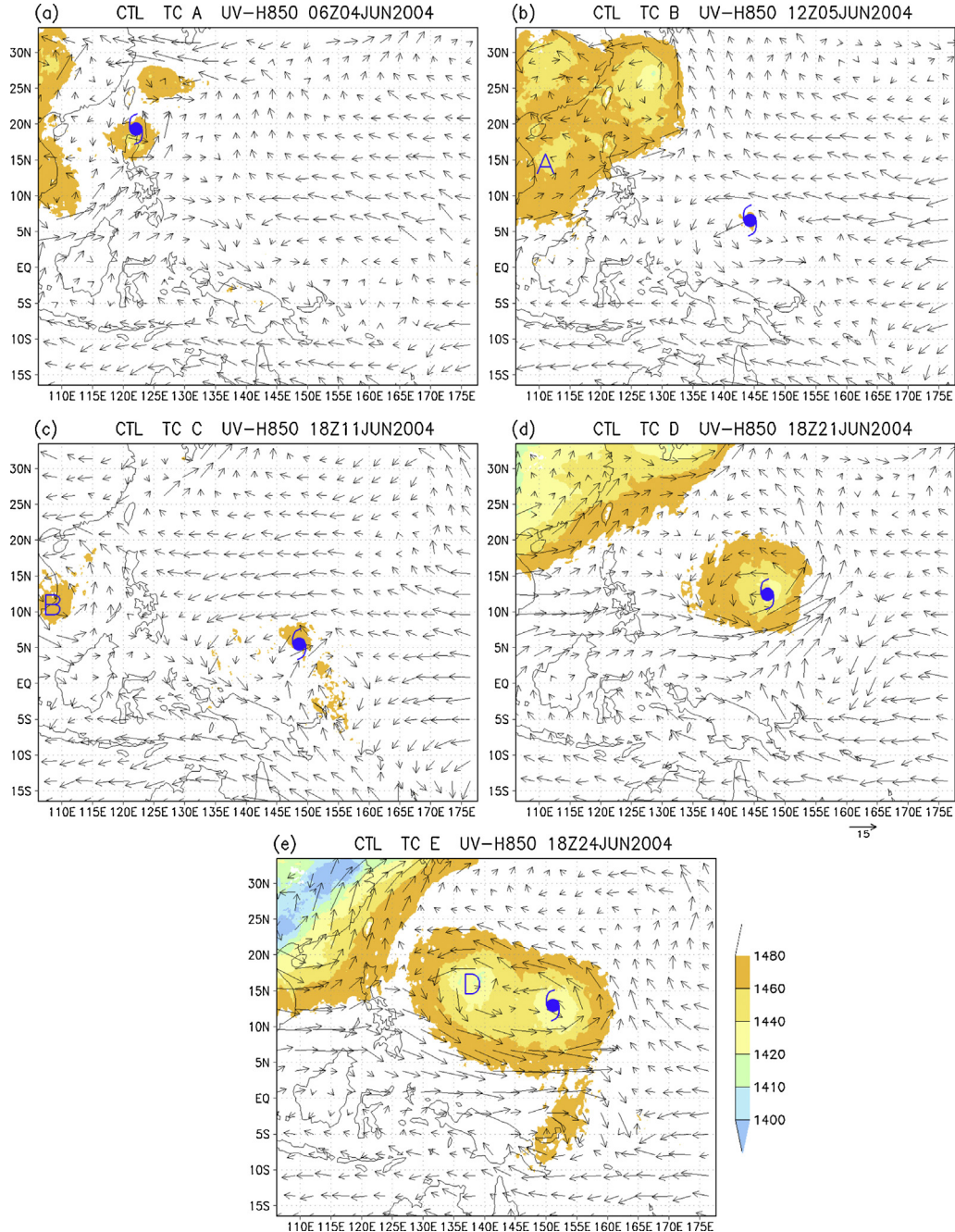


Fig. 4. Same as Fig. 2, but for CTLs of the five TCs.

developing stage of TC A. Although the mean WR indexes show the MJO and MRG-TD wave have positive contribution two days after the warning time (the strengthening stage) of TC A, ER wave is still significant in the strengthening stage of TC A. The value of the mean WR index is 2 times of it in the developing stage of TC A. The mean WR indexes of TC B show that all of three waves are not significant in the developing stage, especially ER wave has negative contribution. After the warning time of TC B, the MRG-TD wave is the most significant wave related to the strengthening stage of TC B. The mean WR index of ER wave (7.94) is the largest in the developing stage of TC C, while the mean WR indexes of other two waves are small. The mean WR index of the MRG-TD wave increases from the developing stage to the strengthening stage of TC C and shows the most significant wave related to the strengthening stage of TC C is the MRG-TD wave. The mean WR indexes of the MRG-TD wave are the largest and exceed ten in the developing (10.21) and strengthening (11.26) stage of TC D, though the mean WR indexes of other two waves are not small. This result shows that the contribution of the MRG-TD wave to TC D development

Table 2

The mean wave-related (WR) index for the three tropical wave disturbances (MJO, ER, MRG-TD) in the developing stage (two days before the warning time) and the strengthening stage (two days after the warning time) of the five TCs. The largest WR indexes of TCs in each stage are denoted in boldface. The negative WR indexes are represented in italic.

		MJO	ER	MRGTD
TC A	Developing stage	−0.82	4.85	−3.86
	Strengthening stage	1.15	8.81	4.10
TC B	Developing stage	1.68	−0.70	1.37
	Strengthening stage	3.12	1.03	4.11
TC C	Developing stage	3.34	7.94	1.57
	Strengthening stage	4.41	5.33	7.51
TC D	Developing stage	5.24	2.74	10.21
	Strengthening stage	5.35	6.31	11.26
TC E	Developing stage	4.59	6.08	−2.52
	Strengthening stage	4.31	5.34	14.56

is significant. In TC E developing stage, ER wave is the most significant wave with the largest WR index (6.08). The mean WR index of the MJO is also large (4.59). The MRG-TD wave has negative contribution in the developing stage of TC E. But the mean WR index of the MRG-TD wave become the largest and exceed fourteen (14.56) in the strengthening stage of TC E, which indicates that the MRG-TD wave dominates when TC E strengthened.

The extended WR index helps us to examine the significant wave related to the developing stage and the strengthening stage of TC. The mean WR indexes of the MJO are all positive, except TC A. Especially the last three TCs (TC C, D, and E) are related to the active MJO envelope in the WNP. ER wave is the most significant wave related to the developing stage of three of five TCs (TC A, C, and E). The MRG-TD wave is only the significant wave related to the developing stage of one TC (TC D). But it is significant in the strengthening stage of all five TCs. This result could be caused by the strong TC disturbance in the strengthening stage and explains that the MRG-TD wave is hard to separate from TCs. Thus, the MRG-TD wave is not considered in the numerical experiments.

The simulated evolutions of TCs in the wave experiments are compared with those of the CTL to assess the effect of waves on TC formation. First, we note that the simulated TCs in the CTL strengthen significantly, demonstrating the model's capability to simulate the growth from initial disturbances to tropical storms. But the model tends to overestimate the strength of TCs compared with the observed TC intensity. In general, regional models tend to overestimate the strength of TC (Yang et al., 2008; Bryan and Rotunno, 2009; Wang and Xu, 2010). Because of TC intensity bias in the model, the definition of model TC intensity needs to be revised accordingly. There are four categories of TCs in the JTWC best track data. A fairly well-defined low-level circulation is classified as a tropical depression (TD) when the maximum sustained wind near the center is between 12.8 and 17.5 m s^{−1} (25–34 knots). The next three categories are TS, typhoon, and super typhoon, defined by V_{\max} thresholds of 17.5, 33, and 66.7 m s^{−1} (34, 64, and 130 knots), respectively. Considering TC intensity bias in the simulated TC development stage, the simulated TCs in all experiments are divided objectively into two categories: nondeveloping TC (TC_n) and developing TC (TS). TC_n is defined as a TC with closed circulation in which the maximum 850 hPa wind speed (V_{\max}) ranges from 12.5 m s^{−1} to 17.5 m s^{−1}, the $120 \times 120 \text{ km}^2$ area-mean vorticity exceeds $5 \times 10^{-5} \text{ s}^{-1}$ and sustains for more than 12 h. A TS is a stronger TC in which the V_{\max} exceeds 17.5 m s^{−1} and the $120 \times 120 \text{ km}^2$ area-mean vorticity exceeds $1 \times 10^{-4} \text{ s}^{-1}$.

4.1. Quantitative measures

Fig. 5 shows the differences of SLP (ΔSLP) and maximum wind (ΔV_{\max}) of initial disturbance between the CTL and each wave experiment at the warning time $H(0)$ for the five TCs. A positive ΔSLP and negative ΔV_{\max} denote a weaker initial disturbance as a result of the missing wave. Therefore, a larger positive ΔSLP and a larger negative ΔV_{\max} indicate a more important influence of the missing wave during the formation stage. The results show an overall strengthening effect by large-scale waves on TC genesis but with two exceptions. First, the simulated TC A becomes stronger when the influence of the MJO is removed (not shown in the figure). That is because the MJO affects not only the development of disturbance, but also the track. More details are to be discussed later. Second, the simulated V_{\max} of TC B in all wave experiments becomes slightly stronger than that in the CTL, showing insignificant contributions from the MJO and ER waves during the development of TC B. More discussion will be shown later.

Fig. 6 shows the differences of SLP and V_{\max} between the warning time $H(0)$ and two day after the warning time $H(48)$ for the five TCs, which are used to measure the intensity change in all simulations. A larger negative ΔSLP with a larger positive ΔV_{\max} (second quadrant) shows the degree of intensification. The mean observed differences are shown in Fig. 6 for reference. Relative to the CTL, the corresponding wave experiments for all TCs show weaker or even negligible growth from $H(0)$ to $H(48)$ except for TC B and TC D. For TC B, the intensification in the noMJO is much stronger than that in the CTL. Similarly, the growth of TC D is stronger in noER and noMJOER than the growth in the CTL. Besides the above, Fig. 6

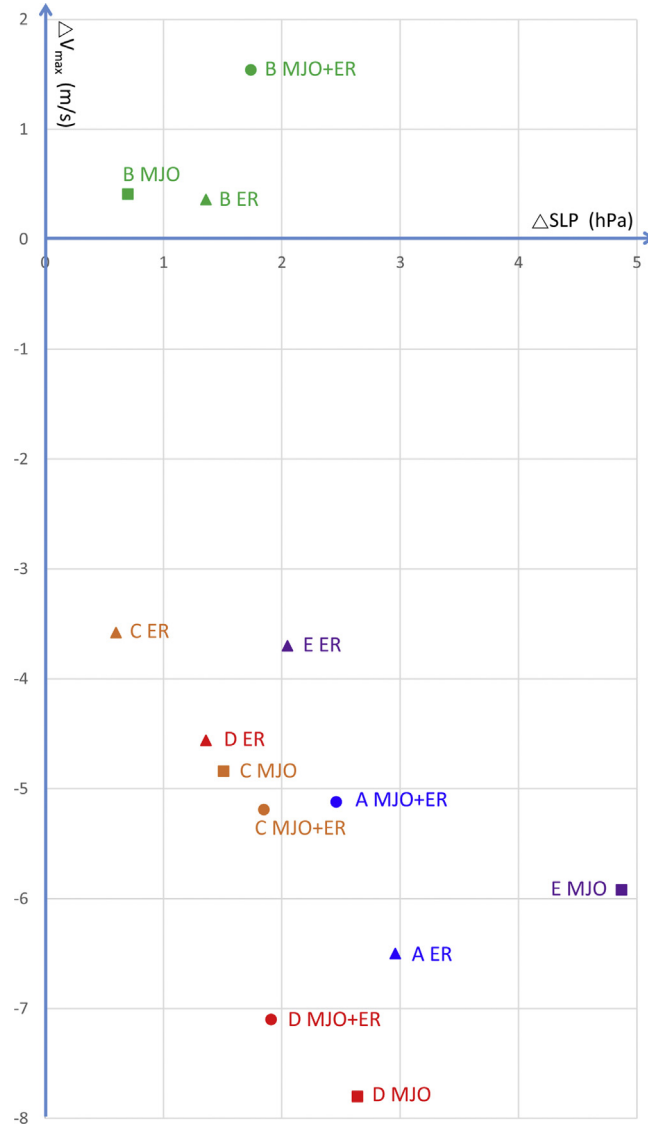


Fig. 5. The differences of SLP (in hPa) and V_{\max} (in $m s^{-1}$) between each wave experiment and the CTL at the warning time for the five TCs. The symbols indicate each experiment. The TC number and the removed wave are marked nearby the corresponding symbols.

further shows that, without the contribution of the MJO, the intensification of all except for TC B is insignificant. The noER experiments for all except for TC B and TC D experience small intensity change. The above results indicate that in general the MJO and ER waves provide a favorable large-scale background for TC intensification. But a systematic examination of the wave–TC relation for each of the five TCs reveals that factors like the MRG–TD waves or local genesis processes must be considered for TC genesis as well. This point is discussed below.

4.2. Assessment for individual TC formation

4.2.1. TC A

The initial disturbance grows into TC A at the north portion of a monsoon gyre, which is a favorable environment for the initial development of TC A. Three days before TC A formed, the initial disturbance exists nearby the cyclonic center of ER waves, which is located east of the Philippines (Figure not shown). The cyclonic circulation of ER waves propagates westward and moves to the west of the Philippines (Fig. 3a). The initial disturbance also moves northwestward into the SCS within the cyclonic circulation of ER waves. The observed large-scale environment suggests that ER wave is an important wave for the initial development of TC A, as the results of WR index (Table 2).

The time series of V_{\max} from all experiments for TC A are shown in Fig. 7a. The time series of each experiment start when the disturbance is defined as a TC_n . The initial disturbance for TC A in the CTL grows slowly in the first 3 days before $H(0)$,

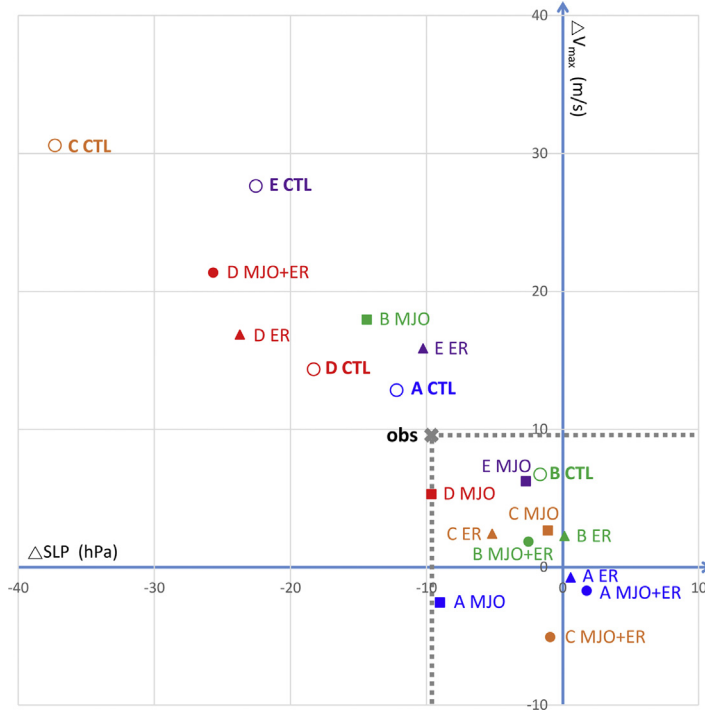


Fig. 6. Intensification of observed and simulated TCs in all wave experiments in terms of ΔSLP and ΔV_{max} between the warning time $H(0)$ and 48 h after the warning time $H(48)$ for the five TCs in June 2004. The gray cross and gray dashed lines indicate the mean observed differences.

but intensifies rapidly from $H(-6)$. Maximum winds in noER and noMJOER remain near 20 m s^{-1} without intensification. The absence of ER waves results in a weakened TC formation (ΔSLP is 2.96 hPa and ΔV_{max} is 6.50 m s^{-1}) at $H(0)$ from the CTL as shown in Fig. 5. But the noMJO experiment shows TC A intensifies significantly with a reduction of SLP (15.03 hPa) and an increase of V_{max} (16.58 m s^{-1}) in noMJO relative to the CTL. The seemingly counter-intuitive results are found to be caused by a different track corresponding to a different steering flow when the MJO is removed as shown in Fig. 8. The track in noMJO shifts eastward relative to the track of TC A in the CTL, due to the lack of easterly anomaly associated with the MJO. TC A goes through the Philippines in the original track but stays over the open ocean in noMJO that allows more air-sea flux exchanges. The heat flux during the developing period in noMJO (159 W m^{-2}) is 50% more than that in the CTL (99 W m^{-2}). The large heat flux from ocean allows the disturbance in noMJO to grow much stronger. Although the easterly anomaly from the MJO is removed in noMJOER, the westerly anomaly from ER waves is also removed. The initial disturbance of TC A in noMJOER still goes through the Philippines and dissipates later (Fig. 8). Removing the MJO and ER waves together result in the largest differences in SLP and V_{max} . The corresponding values are 2.46 hPa and 5.12 m s^{-1} as shown in Fig. 5. The overall results show that ER waves have a dominant influence on TC A formation based on the simulations, consistent with the results of WR index.

4.2.2. TC B

During the formation stage of TC B, the initial disturbance is almost stationary near $145^\circ \text{E}, 6^\circ \text{N}$ (see Fig. 1). The three-day mean winds of low-frequency waves before TC B genesis show a saddle field structure (Figure not shown). The results of WR index indicate that all waves are not significant in the developing stage of TC B. Synthesis of the overall results in CSY10 suggests that TC B is a locally-developed system.

The assessment made in CSY10 is further investigated here through model simulation. First we note that the simulated location of TC B in the CTL is similar to the observation (Fig. 8) while the initial tracks in the three wave experiments turn north-eastward relative to the observation due to the removal of northeasterly wave flow. The intensities of simulated TCs in the CTL and each wave experiment in Fig. 7b do not show much difference. The modeling results support the conclusion made in CSY10 observational analysis that the contributions of waves appear unimportant in the initial development of TC B.

4.2.3. TC C

ER waves are active when TC C formed. The cyclonic and anticyclonic vorticity centers of ER waves are located near 134°E and 159°E , respectively, north of the Equator at TC C warning time (Fig. 3c). Consistent with theoretical ER wave circulation, the convergence is located between the two vorticity centers, where the initial disturbance of TC C developed.

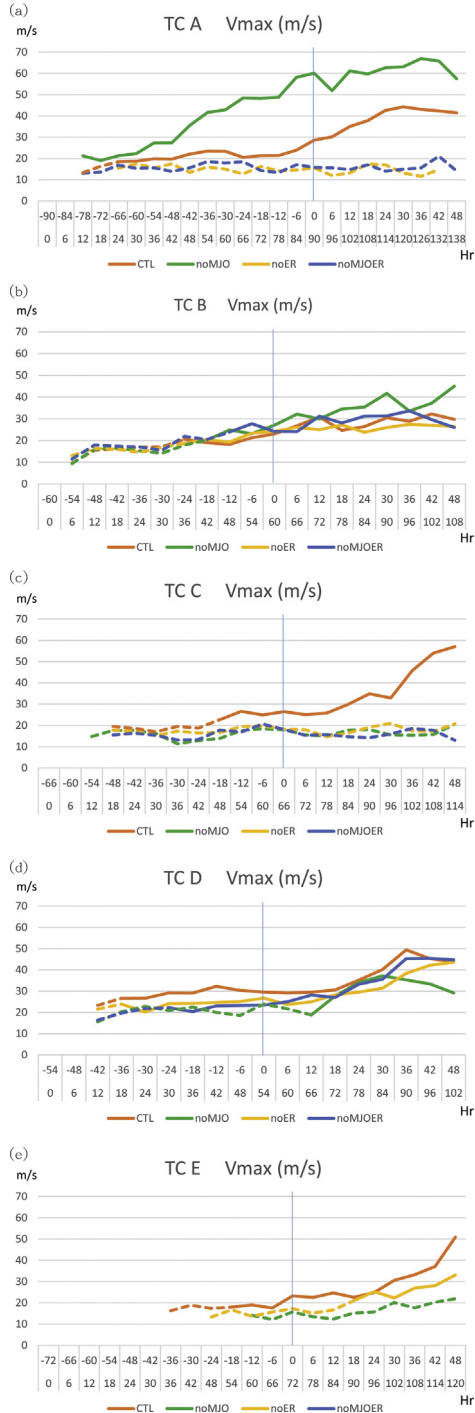


Fig. 7. Time series of V_{\max} (in m s^{-1}) from all experiments for (a) TCA, (b) TC B, (c) TC C, (d) TC D, and (e) TC E. The blue vertical lines indicate the warning time (hour 0) of each TC. The upper horizontal coordinate numbers indicate the times corresponded to the warning time. The lower horizontal coordinate numbers indicate the simulation times. The dashed (solid) lines indicate that the intensity reaches $T\bar{C}_n$ (TS). (For interpretation of the references to color in this figure legend, the reader is referred to the web version of this article.)

The differences of SLP and V_{\max} in Fig. 5 show that all three waves contribute to the formation of TC C with the ΔSLP (1.85 hPa) and ΔV_{\max} (5.19 m s^{-1}) between CTL and noMJOER larger than that of the other two wave experiments. The V_{\max} in CTL increases rapidly after $H(12)$ (Fig. 7c). But the V_{\max} in all wave experiments remain nearly unchanged ($<22 \text{ m s}^{-1}$) through the formation period plus two days after the warning time. The above results show that the MJO and ER waves all provided favorable conditions for TC C formation. Without any of these two waves, the disturbance cannot develop.

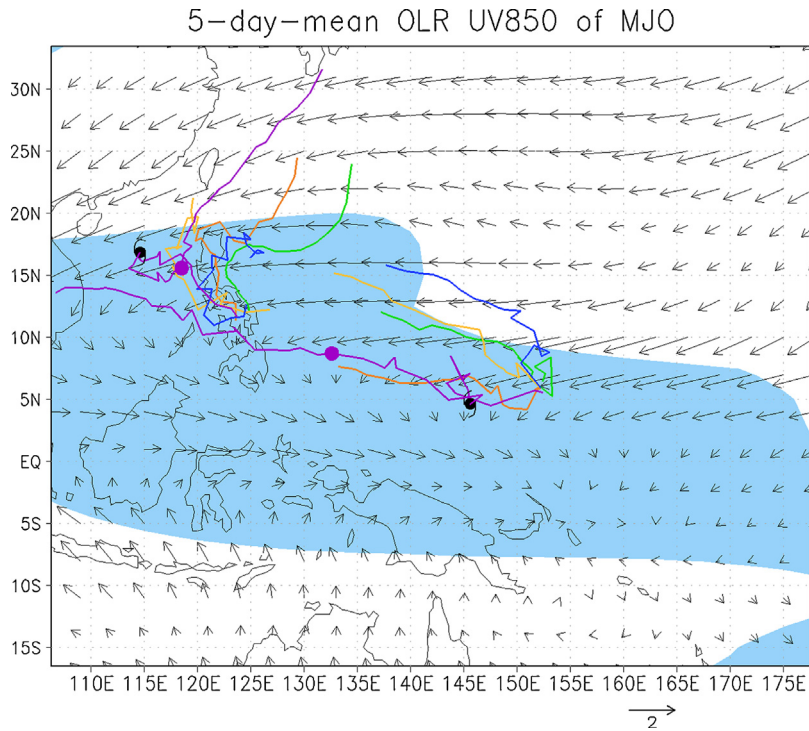


Fig. 8. Observed horizontal structure of space-time filtered winds (vector, in m s^{-1}) at 850 hPa and negative OLR (color shaded) of the MJO averaged from 3 June to 7 June. The group of initial tracks for TC A (near 120° E) and TC B (near 145° E) consists of the track of observation, CTL, noMJO, noER, and noMJOER shown by the purple, orange, green, yellow, and blue tracks, respectively. The observed locations at the warning time $H(0)$ and $H(48)$ are indicated by the Typhoon symbols and circles, respectively. (For interpretation of the references to color in this figure legend, the reader is referred to the web version of this article.)

4.2.4. TCD

Fig. 9 shows the unfiltered streamline and vorticity at 850 hPa four days before TC D formation. The tropical flow field resembles an equatorial MRG wave disturbance with a clockwise circulation centered at 138° E and an anti-clockwise circulation to the east over 150° – 160° E where three vorticity centers exist inside. These three disturbances contract and merge into the initial disturbance of TC D (Figure not show) that moves northwestward and develops into a TD-type disturbance (Fig. 2d).

The observed circulation at the TC D formation time is associated with a cyclonic circulation center of ER waves located at 155° E, 14° N (Fig. 3d) and a MRG-TD wave with dual vorticity cores (Fig. 10). The stronger vorticity center of the MRG-TD wave is located at 138° E, 11° N, accompanied by strong southerly flow at its right side. The initial disturbance of TC D develops west of ER wave low and east of the MRG-TD wave low. The location of low-level convergence zone associated with the MRG-TD wave provides a favorable condition for TC formation. The low-level moisture flux convergence of the MRG-TD wave during the developing period ($3.32 \times 10^{-7} \text{ g kg}^{-1} \text{ s}^{-1}$) is much larger than that of the MJO and ER waves ($0.26 \times 10^{-7} \text{ g kg}^{-1} \text{ s}^{-1}$ and $-0.34 \times 10^{-7} \text{ g kg}^{-1} \text{ s}^{-1}$, respectively). Among all five TCs, the moisture flux convergence associated with MRG-TD wave in TC D is also the largest. The significant contribution of MRG-TD wave on TC D formation is also shown in the results of WR index.

The observed wave train structure of TC D is well simulated in CTL (Fig. 4d). The simulated center of TC D at 147° E, 13° N is just two degree north-east of the observed center. The wave experiments show that missing MJO results in larger differences of SLP and V_{\max} (2.64 hPa and 7.80 m s^{-1}) than that in noER and noMJOER as shown in Fig. 5. Different from other TCs, initial disturbances in all wave experiments intensify to TS (Fig. 7d) after $H(12)$. It is likely that the MRG-TD wave, that is included in the initial condition in all wave experiments, is important for the formation of TC D. Besides the MRG-TD, the combination of the MJO and ER waves also have a significant impact on TC D as shown by the reduction of V_{\max} (7.10 m s^{-1}) and the SLP differences (1.91 hPa) in noMJOER relative to CTL (Fig. 5). The model results indicate that all three waves (MJO, ER, and MRG-TD) contribute significantly to the formation of TC D.

4.2.5. TCE

TC E forms about 1700 km east of TC D when it is located at 135° E, 15° N (Fig. 2e). Because of the close distance and formation time of TC D and TC E, the genesis process of TC E is also influenced by the same ER wave that affects TC D. The circulation at the TC E warning time in Fig. 2e exhibits a twin cyclonic structure symmetric about the Equator, which is similar to the $n=1$ Rossby wave structure. This symmetric structure is also shown in CTL (Fig. 4e), although the simulated

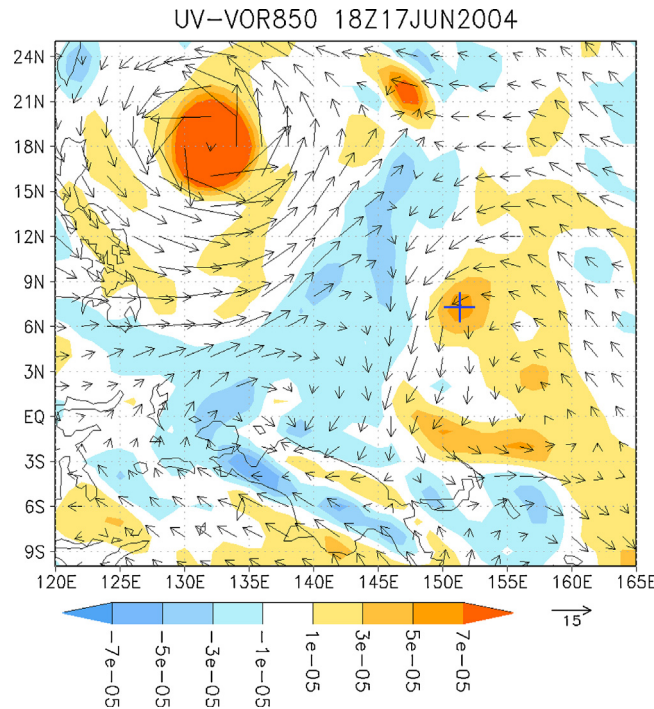


Fig. 9. The unfiltered fields of total winds (vector, in m s^{-1}) and vorticity (color shaded, in s^{-1}) at 850 hPa on 1800UTC June 17 2004. The location of TC D at four days before it formed is indicated by blue cross. (For interpretation of the references to color in this figure legend, the reader is referred to the web version of this article.)

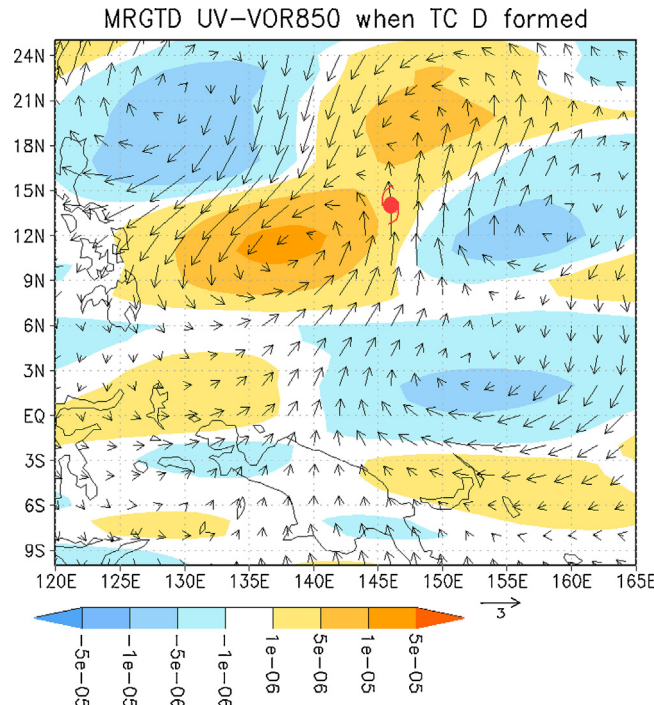


Fig. 10. The observed fields of space-time filtered winds (vector, in m s^{-1}) and vorticity (color shaded, in s^{-1}) of MRG-TD wave at 850 hPa at the warning time of TC D. Typhoon symbols indicate the location of TC D. (For interpretation of the references to color in this figure legend, the reader is referred to the web version of this article.)

Table 3

Summary of simulated TC strength at the end of simulation (48 h after the warning time) in CTL and wave experiments for the five TCs observed in June 2004. TC_n and TS indicate nondeveloping TC and developing TC, respectively. See text for the definitions of TC_n and TS. TS↑ and TS↓ indicate strong and weak TSs, respectively. TC_n and TS↓ are shown with bold.

	CTL	noMJO	noER	noMJOER
TC A	TS	TS↑	TC_n	TC_n
TC B	TS	TS↑	TS	TS
TC C	TS	TC_n	TC_n	TC_n
TC D	TS	TS↓	TS	TS
TC E	TS	TC_n	TS↓	Disappear

TC E and the circulations in Southern Hemisphere are stronger than observation. The simulated TC D is weaker than the observed with a location error about 2°. The flow of TCs D and E together forms a large cyclonic circulation. This cyclonic circulation corresponds to an ER wave (Fig. 3e), centered around 142° E, 15° N. TC E forms east of ER wave, where wave convergence is strong.

The wave experiments show that the initial disturbance in noMJO is weaker than that in CTL (ΔV_{\max} is 4.87 m s⁻¹ and ΔSLP is 5.92 hPa; Fig. 5), and fails to grow into a TS during the whole simulation period. The result indicates a dominant effect of the MJO on TC E formation. The absence of ER waves in noER also weakens the formation of TC E (ΔV_{\max} is 2.05 m s⁻¹ and ΔSLP is 3.70 hPa), but not the eventual intensification into a TS after H(18) although its strength is still weaker than that in CTL. Removing the MJO and ER waves together in noMJOER has a compounding impact on TC formation so that no appreciable disturbance can be recognized. This indicates that TC E formation cannot happen without the MJO and ER waves.

5. Summary and discussion

In this article, we conduct a modeling study to quantitatively assess the contribution of large-scale wave disturbances on TC formation during June 2004. For each of the five TCs formed in the period, we perform four experiments: a control experiment (CTL) and three wave experiments. The CTL is performed with unfiltered analysis data for initial fields and lateral boundary conditions. For the three wave experiments, the Madden Julian oscillations (MJO), equatorial Rossby (ER) waves, and the MJO and ER waves together are respectively removed from the initial fields and lateral boundary conditions. All integrations start from an initial condition prior to the warning time (when the 5° × 5° vorticity embedding the disturbance center is less than the local Coriolis frequency or there is no identifiable close circulation) to 48 h after the warning time.

The effects of large-scale waves on TC formation for the five TCs are summarized in Table 3 that shows the strength of the simulated TCs in all experiments. All five cyclones in the corresponding CTL experiments can intensify to tropical storms. The wave experiments with the MJO removed confirm the results of WR index that the MJO has a significant contribution on the developing disturbance of TCs except for TCs A and B. The genesis locations and initial tracks in noMJO for TCs A and B differ from that of CTL, due to the influence of the MJO flow that changes the air-sea flux exchanges and the strength of the two TCs in the formation period. In addition to the MJO, the different intensities of simulated TCs between CTL and noER also confirm the importance of ER waves for the formation in three of the five TCs. Among three TCs, the initial disturbances of TC A and TC C cannot develop into a TS while the other (TC E) develops into a weaker TS in noER experiments compared to the CTL. Due to a strong synoptic wave contribution (MRG-TD waves), TC D in noER still intensifies into a TS. The combined contribution of the MJO and ER waves to TC formation is more pronounced than the contribution by individual wave alone. For example, the initial disturbance of TC E actually disappears in the noMJOER experiment. Only TC B is not influenced by the MJO, ER waves, or the two combined. The modeling results provide an overall supporting evidence to the observational analysis reported in CSY10.

TC genesis is also sensitive to the location of waves. The previous studies pointed out that the east of wave low where the wave convergence is favorable for tropical cyclogenesis (Molinari et al., 2007; Frank and Roundy, 2006; Dickinson and Molinari, 2002). The same results are also found in our study. The initial disturbances of TC C and TC E developed at the east side of ER wave low (Fig. 3). The initial disturbance associated with the formation of TC D is found to be located at the east side of an MRG-TD wave low (Fig. 10).

The current modeling study provides some quantitative evidence about favorable locations for TC formation in the presence of large-scale wave disturbances. The overall results suggest that the numerical experiments can be useful for investigating the contribution of multi-scale waves on TC formation. Further studies on the interactive mechanism between tropical waves and TC formation in other years and geographical regions can be conducted by using similar modeling approach.

Acknowledgement

We thank Tim Li for useful discussion and all colleague and students who contributed to this study. The research was funded by the National Science Council and Ministry of Science and Technology in Taiwan. L.C. was supported by the NSC

under grants NSC 103-2811-M-002-011. C.H.S. was supported by the MOST under grants MOST 103-2111-M-002-005. M.J.Y. was supported by the MOST under grants MOST 103-2119-M-002-024-MY2. P.L.L. was supported by the NSC under grants NSC 100-2119-M-008-041-MY5.

Appendix I.

In order to understand the influence of different removing fields of waves, three sensitive experiments were designed to remove the influence of thermodynamics fields (noT: height, temperature, and relative humidity fields), kinetic fields (noK: winds fields), and both kinetic and thermodynamics fields (noKT). There is no large difference between CTL and noT (Fig. A1). But the absence of kinetic fields in noK weakens the intensity significantly. The result of noKT is not much different with noK. The results indicate that the influence of kinetic fields is critical. In present study, both kinetic and thermodynamics fields are removed in our wave experiments.

Appendix II.

In our wave experiments, we have to make sure that the space-time filtering is capable of preserving a consistent set of kinetic and thermodynamic fields for selected waves. First, we use the streamfunction of each wave field to obtain the associated height field by solving the nonlinear balance equation (NBE) and then compare it with the filtered height field of the wave. The NBE can be written as

$$\nabla_h^2 \phi = \nabla_h \cdot (f \nabla_h \psi) + 2 \left[\frac{\partial^2 \psi}{\partial x^2} \frac{\partial^2 \psi}{\partial y^2} - \left(\frac{\partial^2 \psi}{\partial x \partial y} \right)^2 \right]$$

where ϕ is the geopotential, ψ is the streamfunction, f is the Coriolis parameter and ∇_h is the horizontal gradient operator (Holton, 2004). Hence, the geopotential height (ϕ/g_0) is interpreted as the balanced height field (H_b), where $g_0 = 9.8 \text{ m s}^{-2}$ is the gravity at mean sea level. The streamfunction is derived from the rotational winds of waves.

The rotational wind and H_b of the MJO at the warning time of TC C are shown in Fig. A2. A large cyclonic circulation accompanied with convection of the MJO is located at the Philippines. Strong easterly north and northeast of the cyclonic circulation corresponds to high H_b . Low H_b is located over the Maritime Continent. The difference fields of wind (divergent winds) and height between the space-time filtered and the “balanced” MJO are shown in Fig. A3. The difference height field ($H_f - H_b$) is about one order of magnitude smaller than H_b , indicating that the kinetic and thermodynamic fields of the filtered wave are near nonlinear balance. But the imbalanced winds in the space-time filtered field accounts for the convergence corresponding to the convective region of the MJO. The easterlies on the eastern part of convergence are accompanied with negative difference heights, which are consistent with the dynamics of the Kelvin wave response (Gill, 1980). The meridional winds on the western part of convergence are consistent with the dynamics of the Rossby wave response.

Fig. A4 shows the rotational wind and H_b of ER waves at the warning time of TC C. The structure of ER wave features cyclonic and anticyclonic circulations around 5° N. The accompanied height field near the Equator is weak. The cyclonic and anticyclonic circulations in the subtropics are more pronounced and are accompanied by strong low and high pressure. Fig. A5 shows the difference fields of wind (divergent winds) and height for ER waves at the warning time of TC C. The convergence (divergence) around TC C occurs east of cyclonic (anticyclonic) circulation and also corresponds to the negative (positive) height anomalies from H_b . The difference height is also one order of magnitude smaller than H_b for ER waves. The result shows that the filtered wave structure not only maintains the balanced kinetic and thermodynamic fields, but also the mutually consistent wave structure in divergent wind and imbalanced height. Both balanced and imbalanced fields are important for driving TC genesis, and it is essential that kinetic and thermodynamic fields of waves are preserved by space-time filtering in numerical experiments.

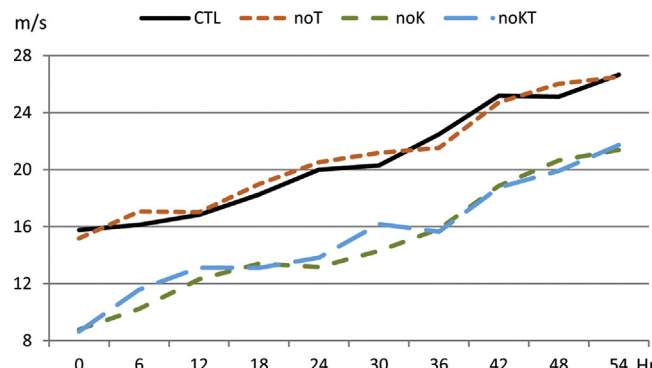


Fig. A1. Time series of V_{\max} (in m s^{-1}) from the sensitivity experiments of different removing fields.

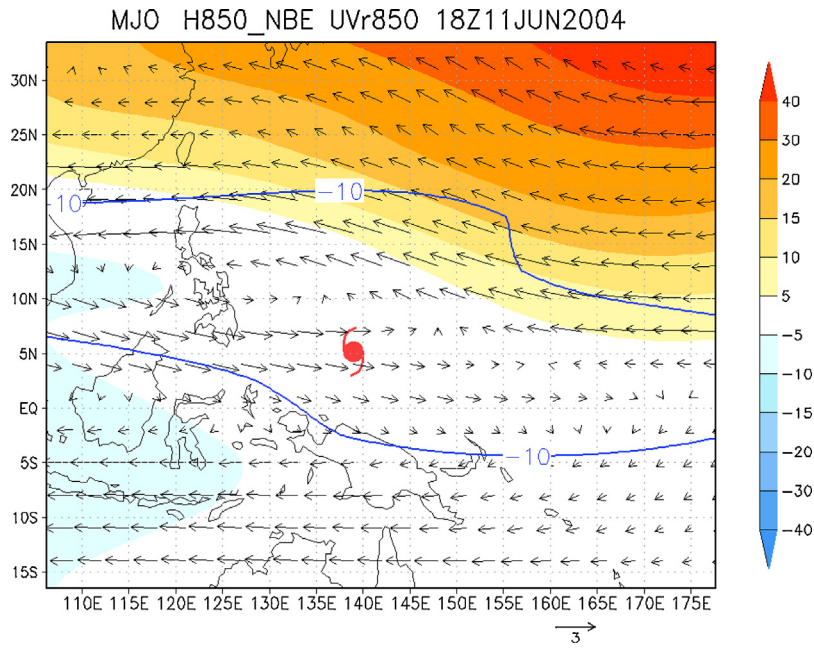


Fig. A2. The horizontal distributions of the balanced geopotential height H_b (color shaded, in m) and the rotational winds (vector, in m s^{-1}) of the MJO at 850 hPa at the warning time of TC C. The blue contours indicate the negative OLR regions of the MJO. Only the OLR value of -10 W m^{-2} is plotted. The genesis location of TC C is indicated by the Typhoon symbols. (For interpretation of the references to color in this figure legend, the reader is referred to the web version of this article.)

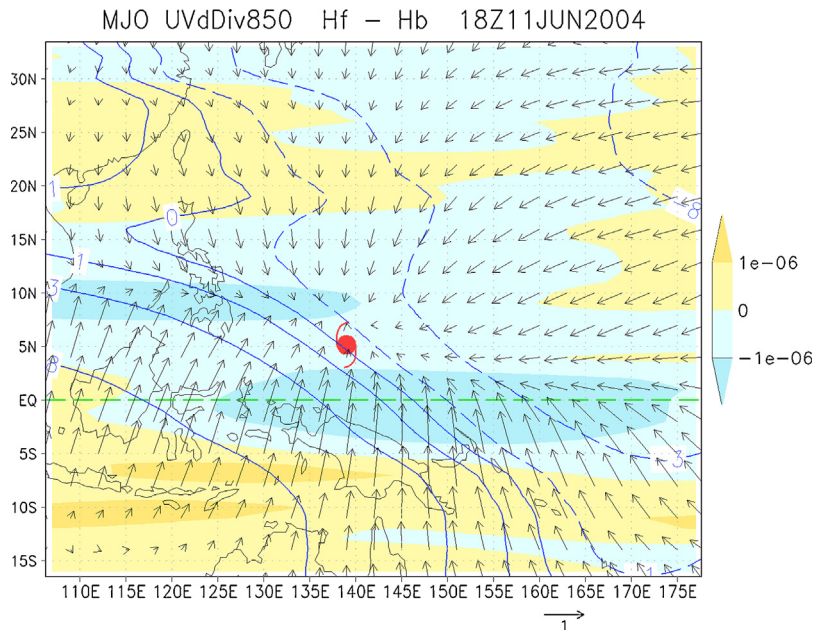


Fig. A3. The horizontal distributions of the divergence fields (color shaded, in s^{-1}) and the divergent winds (vector, in m s^{-1}) of the MJO at 850 hPa at the warning time of TC C. The difference between H_f and H_b is shown in the blue contours (in $-8, -3, -1, 0, 1, 3, \text{ and } 8 \text{ m}$). The genesis location of TC C is indicated by the Typhoon symbols. The green dash line indicates the Equator. (For interpretation of the references to color in this figure legend, the reader is referred to the web version of this article.)

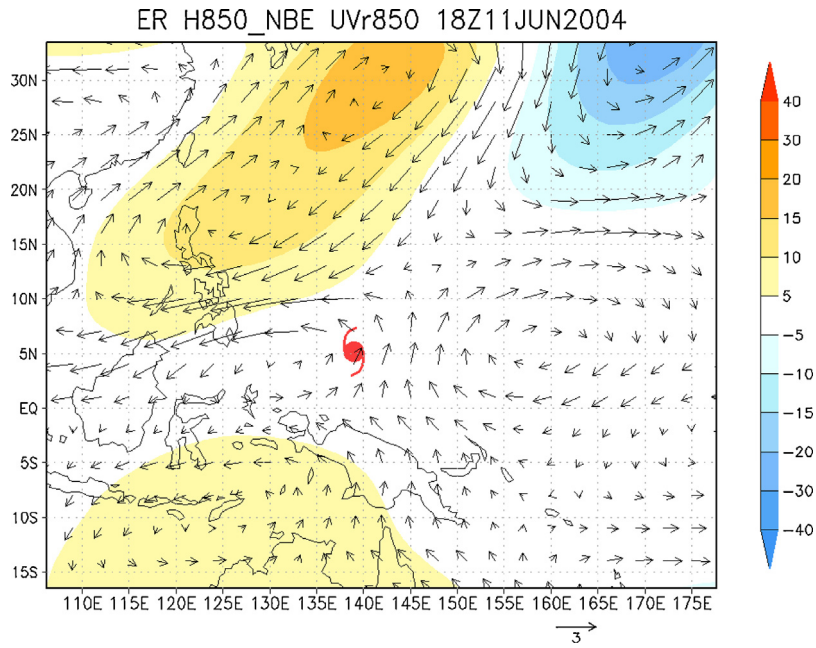


Fig. A4. Same as Fig. A2, but for ER waves.

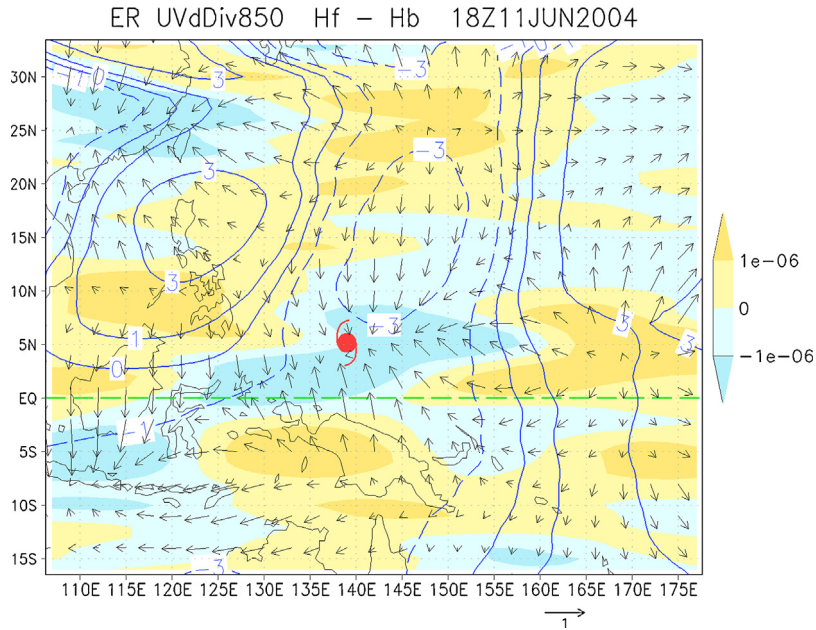


Fig. A5. Same as Fig. A3, but for ER waves.

References

- Bryan, G.H., Rotunno, R., 2009. The maximum intensity of tropical cyclones in axisymmetric numerical model simulations. *Mon. Weather Rev.* **137**, 1770–1789.
- Cao, X., Li, T., Peng, M., Chen, W., Chen, G., 2014. Effects of monsoon trough intraseasonal oscillation on tropical cyclogenesis in the western North Pacific. *J. Atmos. Sci.* **71**, 4639–4660.
- Chang, C.-P., Chen, J.M., Harr, P.A., Carr, L.E., 1996. Northwestward-propagating wave patterns over the tropical western North Pacific during summer. *Mon. Weather Rev.* **124**, 2245–2266.
- Chen, G., Tam, C.Y., 2012. A new perspective on the excitation of low-tropospheric mixed Rossby-gravity waves in association with energy dispersion. *J. Atmos. Sci.* **69**, 1397–1403.
- Ching, L., Sui, C.-H., Yang, M.-J., 2010. An analysis of the multiscale nature of tropical cyclone activities in June 2004: climate background. *J. Geophys. Res.* **115**, D24108, <http://dx.doi.org/10.1029/2010JD013803>.

- Dickinson, M., Molinari, J., 2002. Mixed Rossby-gravity waves and western Pacific tropical cyclogenesis. Part I: Synoptic evolution. *J. Atmos. Sci.* 59, 2183–2196.
- Dudhia, J., 1989. Numerical study of convection observed during the winter monsoon experiment using a mesoscale two-dimensional model. *J. Atmos. Sci.* 46, 3077–3107.
- Frank, W.M., Roundy, P.E., 2006. The role of tropical waves in tropical cyclogenesis. *Mon. Weather Rev.* 134, 2397–2417.
- Fu, B., Li, T., Peng, M., Weng, F., 2007. Analysis of tropical cyclone genesis in the western North Pacific for 2000 and 2001. *Weather Forecast.* 22, 763–780.
- Gall, J.S., Frank, W.M., Wheeler, M.C., 2010. The role of equatorial Rossby waves in tropical cyclogenesis. Part I: Idealized numerical simulations in an initially quiescent background environment. *Mon. Weather Rev.* 138, 1368–1382.
- Gill, A.E., 1980. Some simple solutions for heat-induced tropical circulation. *Q. J. R. Meteorol. Soc.* 106, 447–462.
- Grell, G.A., Devenyi, D., 2002. A generalized approach to parameterizing convection combining ensemble and data assimilation techniques. *Geophys. Res. Lett.* 29, 1693, <http://dx.doi.org/10.1029/2002GL015311>.
- Hendon, H.H., Salby, M.L., 1994. The life cycle of the Madden–Julian oscillation. *J. Atmos. Sci.* 51, 2207–2219.
- Holton, J.R., 2004. *An Introduction to Dynamic Meteorology*. International Geophysics Series, vol. 88., 4th ed. Academic Press, pp. 535.
- Hong, S.-Y., Lim, J.-O.J., 2006. The WRF single-moment 6-class microphysics scheme. *J. Korean Meteorol. Soc.* 42, 129–151.
- Hsu, P.C., Li, T., Tsou, C.-H., 2011. Interactions between boreal summer intraseasonal oscillations and synoptic-scale disturbances over the western North Pacific. Part I: Energetics diagnosis. *J. Climate* 24, 927–941.
- Hsu, P.C., Li, T., 2011. Interactions between boreal summer intraseasonal oscillations and synoptic-scale disturbances over the western North Pacific. Part II: Apparent heat and moisture sources and eddy momentum transport. *J. Climate* 24, 942–961.
- Janjić, Z.I., 2002. Nonsingular implementation of the Mellor–Yamada level 2.5 scheme in the NCEP Meso model. *NCEP Office Note* 437, 61.
- Kanamitsu, M., 1989. Description of the NMC global data assimilation and forecast system. *Weather Forecast.* 4, 335–342.
- Kim, J.-H., Ho, C.-H., Kim, H.-S., Sui, C.-H., Park, S.K., 2008. Systematic variation of summertime tropical cyclone activity in the western North Pacific in relation to the Madden–Julian oscillation. *J. Climate* 21, 1171–1191.
- Lau, K.-H., Lau, N.-C., 1990. Observed structure and propagation characteristics of tropical summertime synoptic scale disturbances. *Mon. Weather Rev.* 118, 1888–1913.
- Lau, K.-H., Lau, N.-C., 1992. The energetics and propagation dynamics of tropical summertime synoptic-scale disturbances. *Mon. Weather Rev.* 120, 2523–2539.
- Lau, K.-M., Chan, P.H., 1986. Aspects of the 40–50 day oscillation during the northern summer as inferred from outgoing longwave radiation. *Mon. Weather Rev.* 114, 1354–1367.
- Li, T., 2006. Origin of the summertime synoptic-scale wave train in the western North Pacific. *J. Atmos. Sci.* 63, 1093–1102.
- Li, T., 2012. Synoptic and climatic aspects of tropical cyclogenesis in western North Pacific. In: Oouchi, K., Fudeyasu, H. (Eds.), *Cyclones: Formation, Triggers and Control*. Nova Science Publishers, pp. 61–94.
- Liang, J., Wu, L., Ge, X., Wu, C.-C., 2011. Monsoonal influence on Typhoon Morakot (2009). Part II: Numerical study. *J. Atmos. Sci.* 68, 2222–2235.
- Liebmann, B., Hendon, H.H., Glick, J.D., 1994. The relationship between tropical cyclones of the western Pacific and Indian Oceans and the Madden–Julian oscillation. *J. Meteorol. Soc. Jpn.* 72, 401–411.
- Liebmann, B., Smith, C.A., 1996. Description of a complete (interpolated) outgoing longwave radiation dataset. *Bull. Am. Meteorol. Soc.* 77, 1275–1277.
- Lindzen, R.D., 1967. Planetary waves on beta-planes. *Mon. Weather Rev.* 95, 441–451.
- Madden, R.A., Julian, P.R., 1971. Detection of a 40–50 day oscillation in the zonal wind in the tropical Pacific. *J. Atmos. Sci.* 28, 702–708.
- Matsuno, T., 1966. Quasi-geostrophic motions in the equatorial area. *J. Meteorol. Soc. Jpn.* 44, 25–43.
- Mlawer, E.J., Taubman, S.J., Brown, P.D., Iacono, M.J., Clough, S.A., 1997. Radiative transfer for inhomogeneous atmospheres: RRTM, a validated correlated-k model for the longwave. *J. Geophys. Res.* 102, 16663–16682.
- Molinari, J., Lombardo, K., Vollaro, D., 2007. Tropical cyclogenesis within an equatorial Rossby wave packet. *J. Atmos. Sci.* 64, 1301–1317.
- Numaguti, A., 1995. Characteristics of 4-to-20-day-period disturbances observed in the equatorial Pacific during the TOGA COARE IOP. *J. Meteorol. Soc. Jpn.* 73, 353–377.
- Reed, R.J., Recker, E.E., 1971. Structure and properties of synoptic-scale wave disturbances in the equatorial western Pacific. *J. Atmos. Sci.* 28, 1117–1133.
- Roundy, P.E., Frank, W.M., 2004. A climatology of waves in the equatorial region. *J. Atmos. Sci.* 61, 2105–2132.
- Schreck, C.J., Molinari, J., Mohr, K.I., 2011. Attributing tropical cyclogenesis to equatorial waves in the western North Pacific. *J. Atmos. Sci.* 68, 195–209.
- Takayabu, Y.N., Nitta, T., 1993. 3–5 day-period disturbances coupled with convection over the tropical Pacific Ocean. *J. Meteorol. Soc. Jpn.* 71, 221–246.
- Takayabu, Y.N., Nitta, T., 1994. Large-scale cloud disturbances associated with equatorial waves. Part I: Spectral features of the cloud disturbances. *J. Meteorol. Soc. Jpn.* 72, 433–449.
- Wallace, J.M., Kousky, V.E., 1968. Observational evidence of Kelvin waves in the tropical stratosphere. *J. Atmos. Sci.* 25, 900–907.
- Wang, B., Rui, H., 1990. Synoptic climatology of transient tropical intraseasonal convection anomalies: 1975–1985. *Meteorol. Atmos. Phys.* 44, 43–61.
- Wang, Y., Xu, J., 2010. Energy production, frictional dissipation, and maximum intensity of a numerically simulated tropical cyclone. *J. Atmos. Sci.* 67, 97–116.
- Wheeler, M., Kiladis, G.N., 1999. Convectively coupled equatorial waves: analysis of clouds and temperature in the wavenumber-frequency domain. *J. Atmos. Sci.* 56, 374–399.
- Wu, L., Liang, J., Wu, C.-C., 2011. Monsoonal influence on Typhoon Morakot (2009). Part I: Observational analysis. *J. Atmos. Sci.* 68, 2208–2221.
- Xu, Y., Li, T., Peng, M., 2014. Roles of synoptic-scale wave train, intraseasonal oscillation, and high-frequency eddies in genesis of Typhoon Manyi (2001). *J. Atmos. Sci.* 71, 3706–3722.
- Yamazaki, N., Murakami, M., 1989. An intraseasonal amplitude modulation of the short-term tropical disturbances over the western Pacific. *J. Meteorol. Soc. Jpn.* 67, 791–807.
- Yanai, M., Maruyama, T., 1966. Stratospheric wave disturbances propagating over the equatorial Pacific. *J. Meteorol. Soc. Jpn.* 44, 291–294.
- Yang, M.-J., Zhang, D.-L., Huang, H.-L., 2008. A modeling study of typhoon Nari (2001) at landfall. Part I: Topographic effects. *J. Atmos. Sci.* 65, 3095–3115.